Results in Chemistry 6 (2023) 101032

Contents lists available at ScienceDirect

Results in Chemistry

journal homepage: www.sciencedirect.com/journal/results-in-chemistry

N-Substituted 3-Aminooxindoles and *N*-Propargyl Derivatives: Potential Biological Activities against Alzheimer's Disease

Tereza Hofmanova [a,b,c,1], Carolina Marques [a,1], Alfonso T. García-Sosa [d], Óscar López [e], Luisa Leitzbach [f], Elisabete P. Carreiro [a], Aday González-Bakker [f], Adrián Puerta [f], Holger Stark [g], José M. Padrón [f], José G. Fernández-Bolaños [e], Anthony J. Burke [a,b,h,i,j,*]

[a] *LAQV-REQUIMTE, University of Évora, Institute for Research and Advanced Studies, Rua Romão Ramalho, 59, 7000-671 Évora, Portugal*
[b] *Chemistry and Biochemistry Department, School of Science and Technology, University of Évora, Rua Romão Ramalho 59, 7000-671 Évora, Portugal*
[c] *Department of Chemistry, Faculty of Science, University of Hradec Králové, Rokitanského 62, 50003 Hradec Králové, Czech Republic*
[d] *Institute of Chemistry, University of Tartu, Ravila 14 A, Tartu 50411, Estonia*
[e] *Departamento de Química Orgánica, Facultad de Química, Universidad de Sevilla, Apartado 1203, E-41071 Seville, Spain*
[f] *BioLab, Instituto Universitario de Bio-Orgánica "Antonio González" (IUBO-AG), Universidad de La Laguna, c/ Astrofísico Francisco Sánchez 2, E-38206 La Laguna, Spain*
[g] *Heinrich Heine University Düsseldorf, Institute of Pharmaceutical and Medicinal Chemistry. Universitaetsstr. 1, 40225 Duesseldorf, Germany*
[h] *Faculty of Pharmacy, University of Coimbra, Pólo das Ciências da Saúde, Azinhaga de Santa Comba, 3000-548 Coimbra, Portugal*
[i] *Centro de Química de Coimbra, Institute of Molecular Sciences, Departamento de Química, Faculdade de Ciências e Tecnologia, Universidade de Coimbra, 3004-535 COIMBRA, Portugal*
[j] *Center for Neurosciences and Cellular Biology (CNC), Polo I, Universidade de Coimbra Rua Larga Faculdade de Medicina, Polo I, 1°andar, 3004–504, Coimbra, Portugal*

ARTICLE INFO

Keywords:
Oxindole
Alzheimer's disease
Cholinesterase
Mono-amine oxidase
Molecular docking
STD-NMR
Continuous live cell imaging

ABSTRACT

The oxindole core is an important structural motif in many natural and synthetic substances with various biological activities including anticancer, antineurodegenerative, and antimicrobial properties. This report focuses on the synthesis and biological activity of a series of novel *N*-substituted 3-aminooxindoles and their assessment in cholinesterase (ChE) and monoamine oxidase (MAO) inhibition. With regard to MAO inhibition, a series of *N*-propargyl containing derivatives was synthesized and screened. Despite being weak inhibitors of MAO-A and MAO-B, the compounds were selective for butyrylcholinesterase (BuChE) over acetylcholinesterase (AChE). Most of them were strong inhibitors of BuChE with IC_{50}s of less than 1 μM, and one compound showed an $IC_{50} = 27$ nM. The mechanism of action of the inhibition was pin-pointed through molecular modeling, and was validated using saturation-transfer-difference (STD) NMR. Some of the compounds were screened for anti-oxidant properties, but showed no activity. The same compounds were screened in the neurodegenerative disease model cell-line SH-SY5Y and although some were found to be non-cytotoxic, others were moderately cytotoxic. Continuous live cell imaging experiments showed that the compounds do not induce relevant cell damage and thus, the compounds might be interesting drug candidates for Alzheimer's disease. Furthermore, the most active compounds showed excellent drug-likeness and pharmacological properties predicted using Swiss-ADME, and the pharmacokinetic simulations indicated that all these compounds cross the blood-brain-barrier.

Introduction

Alzheimer's disease (AD) is a neurodegenerative disorder that impairs mental ability and interrupts neurocognitive function. This neuropathological condition is highlighted by neurodegeneration, neural loss, and the development of both neurofibrillary tangles and amyloid beta (Aβ) plaques [1].

Effective treatments for AD are inexistent, with no known disease-

* Corresponding author at: LAQV-REQUIMTE, University of Évora, Institute for Research and Advanced Studies, Rua Romão Ramalho, 59, 7000-671 Évora, Portugal.
E-mail address: ajburke@ff.uc.pt (A.J. Burke).
[1] Both authors have contributed equally to this work.

https://doi.org/10.1016/j.rechem.2023.101032
Received 15 June 2023; Accepted 3 July 2023
Available online 8 July 2023

modifying solutions despite the best efforts by the scientific and medical communities. The few drugs available on the market show only symptomatic relief (Fig. 1), except for the new β-amyloid level lowering antibody known as lecanemab, developed by Eisai and Biogen, which was granted accelerated approval by the FDA in January 2023 [2,3]. The causes of AD are not fully understood. In the β-amyloid hypothesis, the presence of $A\beta_{40}$ aggregates and tau protein fibrils are considered to be the primary pathological source of AD [1]. However, there are strong indications that AD is a multifactorial ailment, that involves other factors like neuroinflammation, acetylcholine degradation (the cholinergic hypothesis), glial cell dysfunction, increased tau phosphorylation, deregulation of calcium metabolism, enhanced glycogen-synthase kinase (GSK)-3β activity, stimulation of cell death or neuronal apoptosis and oxidative stress [4]. Moreover, various drug candidates targeting these pathological processes were unsuccessful in preclinical or clinical trials, perhaps because of their low bioavailability, blood–brain-barrier penetration, and rapid drug excretion in such treatments. Therefore, the development of new small molecule disease-modifying therapies is essential. With respect to the cholinergic hypothesis (the most successful approach to date), the three prescribed drugs currently on the market include: donepezil, rivastigmine, and galantamine (the first two are selective acetylcholinesterase (AChE) inhibitors and the latter is a dual AChE/butyrylcholinesterase (BuChE) inhibitor).

The oxindole core is a unit present in many natural products and bioactive compounds [5]; some examples include: nintedanib [6] (interstitial lung ailments like idiopathic pulmonary fibrosis (IPF) treatment), sunitinib (tyrosine kinase inhibitor, used to treat drug gastrointestinal stromal tumors and renal cell carcinoma) [7], SSR-149414 (an orally active nonpeptide vasopressin-receptor antagonist) [8], and NITD609 (an antimalarial drug candidate) [9] (Fig. 2**A**–**D**).

Moreover, oxindole-containing molecules have also been shown to be very good ChE inhibitors. One specific example includes the drug tenidap (Fig. 2**E**) which through a combination of cyclooxygenase inhibition and cytokine modulation, leads to a slowing of plaque formation and neuronal damage [10]. With regards to BuChE inhibition we have shown that 3-hydroxyoxindoles can be potent BuChE inhibitors (in the range 1–10 μM) [12–14]. Also a number of potent 3-aminospirooxindole BuChE inhibitors, including tenidap, have demonstrated very good BuChE inhibitions [11,15,16]. Moreover, we also developed selective BuChE inhibiting 2-oxindole-3-carboxamides (in all cases they showed low potency for AChE) (Fig. 3) [17].

Monoamine oxidase A and B (MAO-A and B) inhibition has also been a strategy for treating both AD and Parkinson's disease (PD) [18]. These MAOs are FAD associated enzymes found on the mitochondrial outer membrane. Whilst MAO-A catalyzes the oxidative deamination of serotonin, adrenaline and noradrenaline, MAO-B is known to preferentially deaminate β-phenethylamine and benzylamine. Some of the most potent MAO inhibitors, like; rasagiline, selegiline and clorgyline, contain an *N*-propargyl unit, which has been considered to be the key pharmacophore that inhibits MAO via a covalent interaction with the FAD unit [19]. The introduction of a propargyl group on the 3-amino unit (and other oxindole scaffold positions) would provide interesting rasagiline analogues (see Scheme 3) that could be active against MAO-A and/or B. Rasagline (Scheme 3) is a well-known commercial irreversible MAO-B inhibitor.

In this article we discuss our efforts in developing free and Boc (*tert*-butoxycarbonyl) protected 3-aminooxindole derivatives, transforming them into *N*-propargyl derivatives and studying their potency for both BuChE and MAO inhibition.

Results and discussion

Chemistry

In 2016 we reported a novel synthetic methodology for the synthesis of a library of 3-amino-aryl-oxindole derivatives containing an *N*-methyl group in the isatin core **(2a-k)**, **(3a-k)** and **(4a-i)**, *via* a rhodium-catalyzed arylation of *N*-Boc-protected ketimines (Scheme 1) [20] [the synthesized compounds described in this report were not biologically assayed]. It also became of interest to us, for comparative purposes, to prepare a series of *N*-benzyloxindole analogues **(5a-h)** and **(6a-c)** using the same reported reaction conditions and with the isatin-derived *N*-Boc-protected ketimines **(1d)** and **(1e)** (Scheme 1). This was partly due to the fact that the *N*-benzyl group is an important pharmacophoric unit present in donepezil (Fig. 1**A**) and is also known to be an important pharmacophore for MAO inhibition [18,21]. The overall yields were moderate to very good and no significant differences were observed in the isolated yields for *N*-Me and *N*-benzyl oxindole products (Scheme 1).

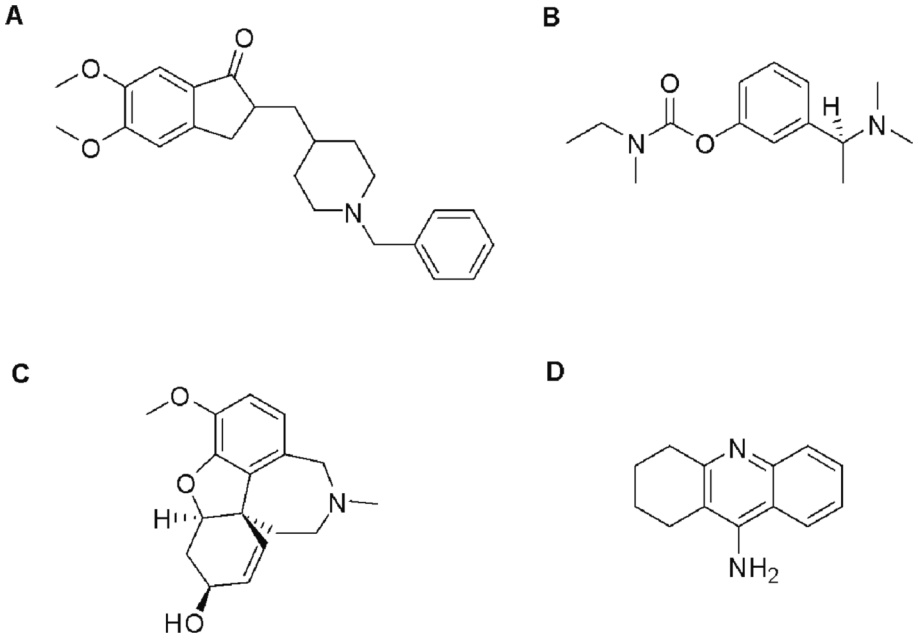

Fig. 1. Approved drugs for AD treatment: donepezil (A), rivastigmine (B), galantamine (C), and tacrine (D) (due to chronic hepatotoxicity, this drug has been removed from the market).

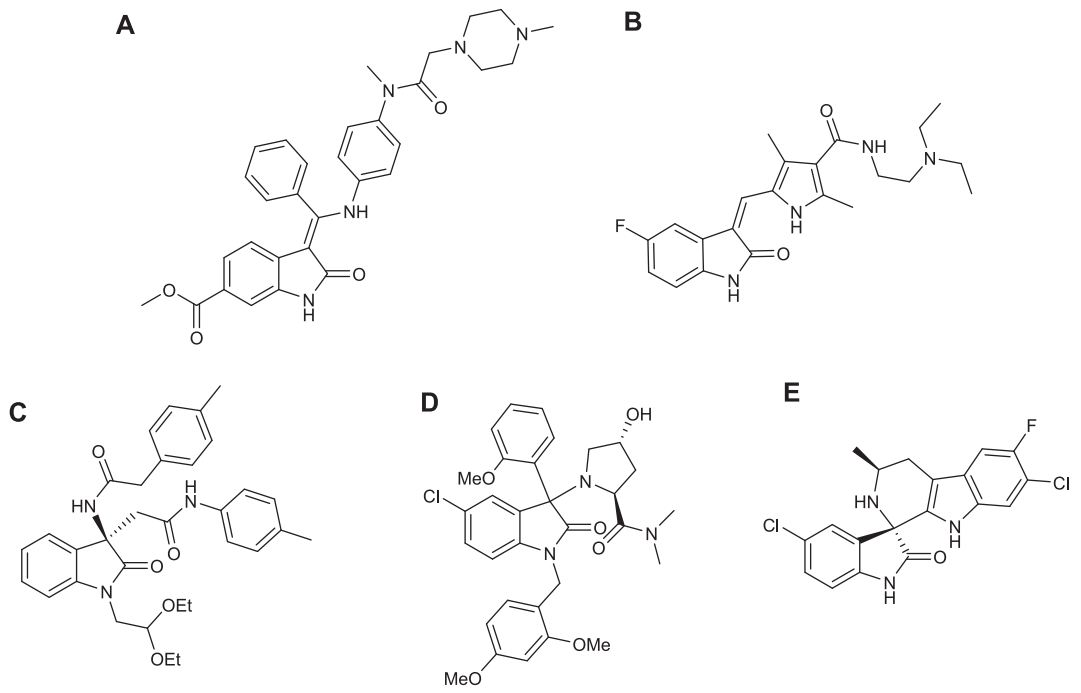

Fig. 2. Examples of biologically active oxindoles: nintedanib (A) [6], sunitinib (B) [7], SSR-149415 (C) [8], NITD609 (D) [9] and tenidap [10].

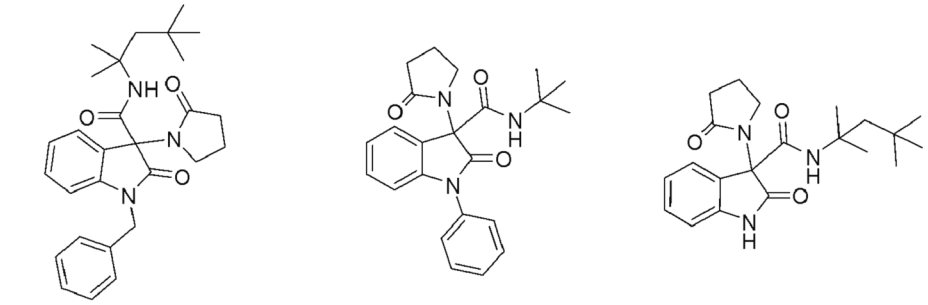

Fig. 3. Selected 2-oxindole-3-carboxamides as potential inhibitors of ChEs [17].

Compounds **(2c)**, **(3c)**, **(4a-b)**, **(5c)**, and **(6b-c)** gave the best reaction yields (>80% isolated yield, Scheme 1). Attempts to synthesize the *N*-benzyl-5-bromo-*N*-Boc-protected ketimine were unsuccessful as only the *N*-Boc-protected ketimine **(1d)** was isolated, in 57% yield, proving that the C5-Br bond was cleaved during the reaction.

The deprotection of the *N*-Boc group was fully demonstrated using the previously optimized reaction conditions [20], using trifluoroacetic acid (TFA) in CH_2Cl_2, at room temperature (Scheme 2). A new family of free 3-amino-aryl-oxindole derivatives **(7)** (Scheme 2) was obtained in generally moderate yields (10 to > 99% yield) and also biologically assayed. The best yields were recorded for compounds **(7l)** and **(7n)** with > 99% and 70% yield, respectively (Scheme 2). Oxalyl chloride was also studied, but was found to be too harsh, although the isolation of the free amine was easier than using TFA and the product obtained in acceptable purity.

These deprotected compounds (Scheme 2) were then transformed into a variety of *N*-propargylated derivatives, using the method recently developed in our laboratory [21].

Seven new 3-amino-aryl-oxindole hybrids with propargyl units attached at position 3 **(11a-d)** and position 5 **(10a-c)** of the isatin-oxindole framework were successfully obtained (Scheme 3). The copper-catalyzed route to primary aromatic amines from aromatic halides using sodium azide was one of the reactions used to afford compounds **(9a)** and **(9b)**.

Biological evaluation

In vitro cholinesterase inhibitory activity

Tables 1 and 2 show the screening results of our non-propargylated compounds against *ee*AChE and *eq*BuChE. Ketimine **(1d)** was found to be a potent *ee*AChE inhibitor and even more so, for *eq*BuChE (IC_{50} = 11 and 2.30 μM, respectively; Table 1, entry 1). The *N*-methyl substituted 3-aminooxindoles can be split into four subgroups - the subgroup with a non-substituted oxindole skeleton **(2a)-(2k) (Group MetA)**, a 5-Br substituent **(3a)-(3k) (Group MetB)**, a 5-Me substituent **(4a)-(4i) (Group MetC)** and the free amine analogues **(7 l)-(7o) (Group MetD)**. In the case of the *N*-benzyl analogues, they were divided into three groups; unsubstituted **(5a)-(5h) (Group BnA)**, with the 5-Me substituent **(6a)-(6c) (Group BnB)** and the free-amines **(7a)**, **(7i)**, **(7j)**, **(7m)**, **(7n)** and **(7o) (Group BnC)**.

All the compounds, except **(1d)** showed very low inhibitory potencies against *ee*AChE with IC_{50} values > 50 μM. Interestingly, they

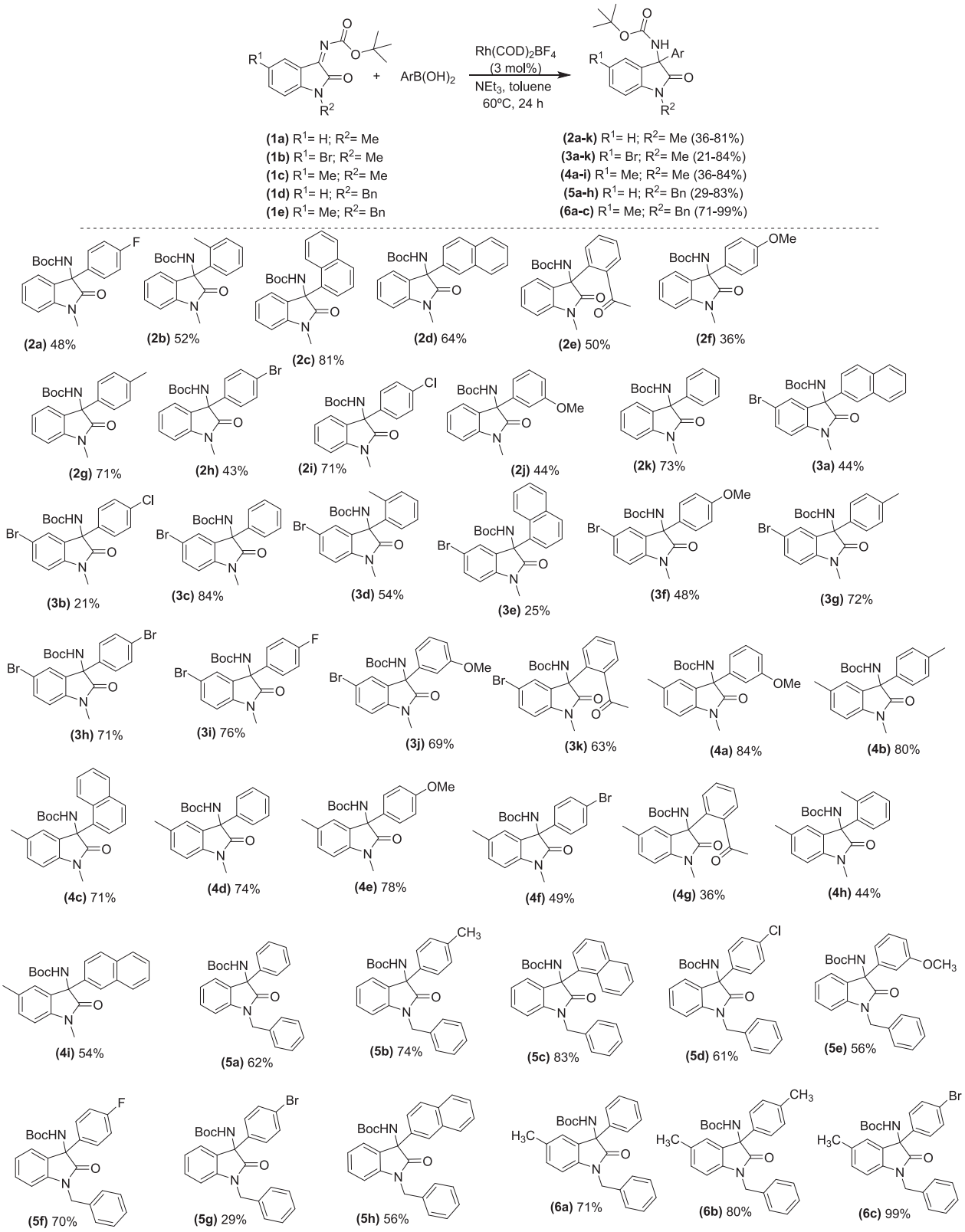

Scheme 1. Rh-Catalyzed synthesis of *N*-Boc-3-amino-3-aryl-oxindole derivatives (2)-(6) from isatin-derived *N*-Boc-protected ketimines (1).

were selective for *eq*BuChE. In the subgroup **(Group MetA)**, **(2a-2j)**, only **(2c)** (Table 1, entry 4) could reach submicromolar inhibition concentrations (0.29 μM) for BuChE. The others were either devoid of relevant activity at the highest tested concentration (IC_{50} > 50 μM) or showed moderate inhibition (IC_{50} = 22–50 μM). In the case of **(Group MetB) (3a-3 k)** both compounds **(3e** and **3f)** gave inhibition levels lower than 8.0 μM and **(3i)** gave an IC_{50} of 11.0 μM against BuChE. In the case of **(Group MetC)**, the observed low IC_{50} values indicated the importance of the 5-Me group over the 5-Br, for example, compounds **(4c)**, **(4e)**, **(4f)**, and **(4i)** gave values of less than 9.0 μM. In the case of the *N*-benzyl

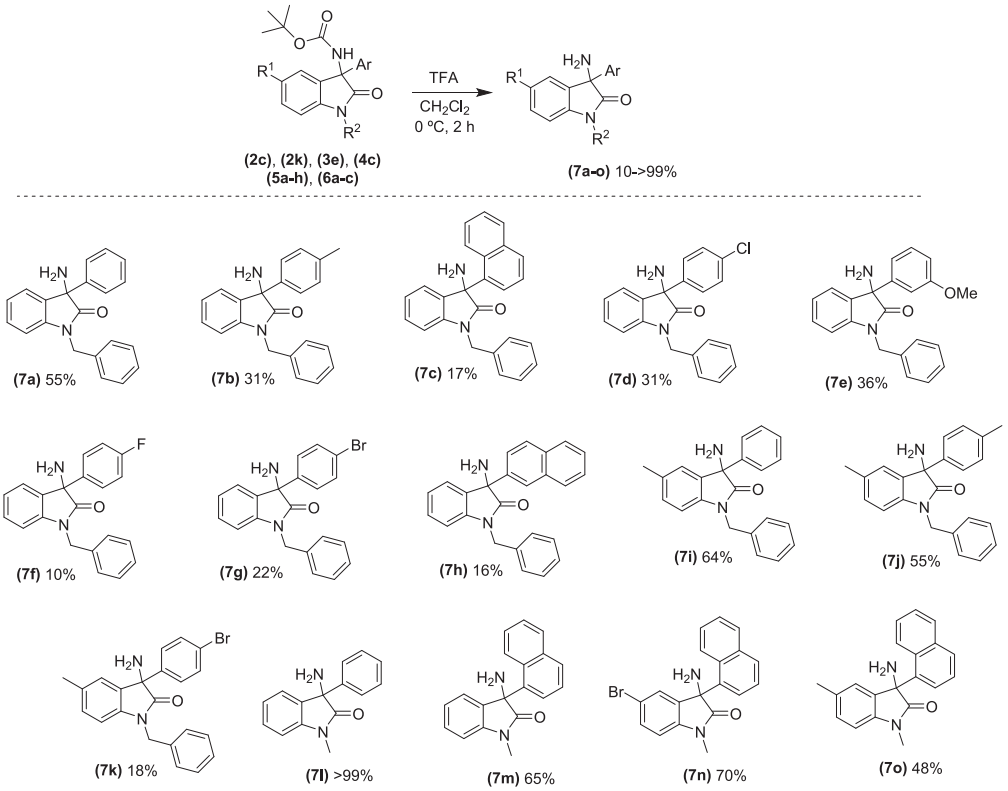

Scheme 2. Synthesis of the free 3-amino-aryl-oxindole derivatives (7).

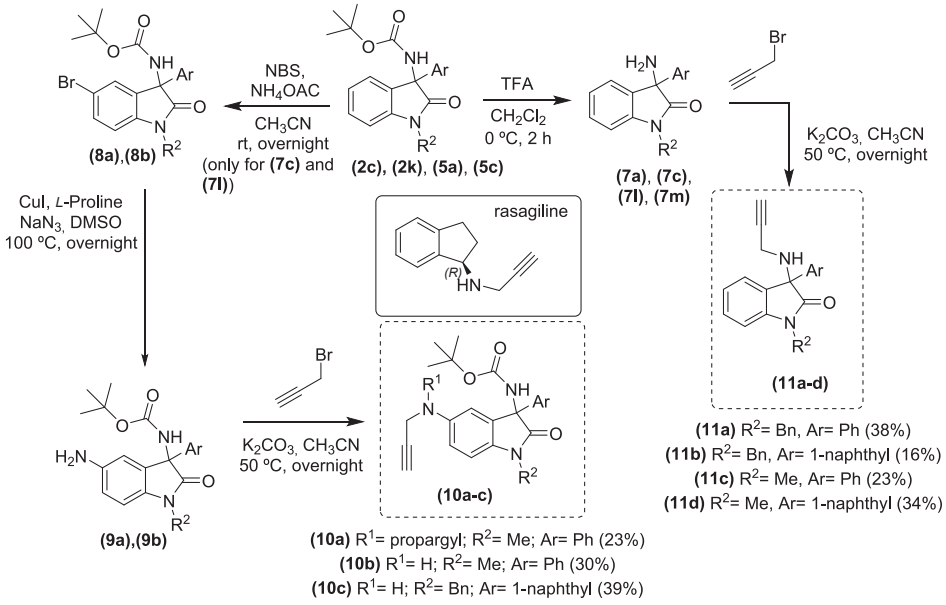

Scheme 3. Synthesis of the propargylated amino-oxindole hybrids (**10a-c**) and (**11a-d**). NBS: *N*-bromosuccinimide.

substituted molecules, **(Group BnA)** and **(Group BnB) (5a)-(5 h)** and **(6a)-(6c)**, even more potent inhibitions were observed, with all values below 4.0 μM and, and remarkably, compound **(5c)** was potent down to 27.0 nM, roughly 204-fold more potent than the drug galantamine, used herein as a positive control. This latter result was most probably due to the size and the aromatic nature of the compound allowing it to interact favorably with aromatic units within the BuChE active site like: Trp82, Trp231 and Phe329. **(Group BnC)** also furnished some very good levels of inhibition of not>18 μM and most of them had values lower than 10 μM.

The free amine analogues **(7a)**, **(7i)**, **(7j)**, **(7m)**, **(7n)** and **(7o)** showed potencies of between 1.0 and 18.0 μM (Table 1). With the exception of **(7i)**, the *N*-methyl analogues were the most potent ones in this class. Moreover, the absence of the Boc group did not make a substantial difference to the inhibition. It is noteworthy to say that for BuChE inhibition, most of these compounds were more potent than the benchmark, galantamine [22].

With regard to the mechanism of inhibition, we looked at two of our

Table 1
IC_{50} values (μM) for *ee*AChE and *eq*BuChE of selected compounds.

Compound	*ee*AChE (μM)[a]	*eq*BuChE (μM) [a]	Compound	*ee*AChE (μM)[a]	*eq*BuChE (μM) [a]
(1d)	11 ± 2	2.3 ± 0.0	**(4d)**	>50	23.0 ± 1.0
(2a)	>50	>50	**(4e)**		8.9 ± 0.5
(2b)		>50	**(4f)**		5.9 ± 0.8
(2c)		0.29 ± 0.04	**(4 g)**		27.0 ± 1.0
(2d)		22.0 ± 6.0	**(4 h)**		>50
(2e)		>50	**(4i)**		3.4 ± 0.9
(2f)		>50	**(5a)**		1.1 ± 0.0
(2 g)		>50	**(5b)**		1.3 ± 0.0
(2 h)		38.0 ± 4.0	**(5c)**		0.027 ± 0.000
(2i)		50.0 ± 0.0	**(5d)**		3.9 ± 0.6
(2j)		>50	**(5e)**		0.89 ± 0.16
(3a)		>50	**(5f)**		3.5 ± 0.3
(3b)		18.0 ± 1.0	**(5 g)**		0.91 ± 0.14
(3c)		44.0 ± 1.0	**(5 h)**		0.62 ± 0.04
(3d)		>50	**(6a)**		2.2 ± 0.1
(3e)		7.3 ± 1.1	**(6b)**		0.86 ± 0.03
(3f)		7.7 ± 0.6	**(6c)**		1.4 ± 0.1
(3 g)		39.0 ± 2.0	**(7a)**		12.0 ± 1.0
(3 h)		>50	**(7i)**		18.0 ± 1.0
(3i)		11.0 ± 2.0	**(7j)**		1.0 ± 0.1
(3j)		23.0 ± 1.0	**(7 *m*)**		7.4 ± 0.7
(3 k)		20.0 ± 0.0	**(7*n*)**		2.4 ± 0.0
(4a)		24.0 ± 3.0	**(7o)**		2.7 ± 0.4
(4b)		24.0 ± 1.0	**Galantamine**[b]	1.3 ± 0.1	5.5 ± 0.4
(4c)		1.9 ± 0.1			

[a] Average of 5–9 different inhibitor concentrations and data obtained in duplicate, expressed as the mean ± SD. Substrate concentrations were fixed at 121 μM for AChE and 112 μM for BuChE. Data are expressed as mean ± standard deviation.
[b] Positive control.

Table 2
Kinetic parameters[a] for *eq*BuChE inhibition for the best compounds.

Compound	K_{ia} (μM)	K_{ib} (μM)	Inhibition mode
(2c)	0.82 ± 0.10	3.5 ± 0.5	Mixed
(5c)	0.019 ± 0.003	0.065 ± 0.005	Mixed

[a] 5 different substrate concentrations were used (¼ Km – 4 Km), and 4 different inhibitor concentrations. Cornish-Bowen plots were used for calculating the kinetic parameters.

best BuChE inhibitors, namely, **(2c)** and **(5c)**, and we found that they were both efficient mixed inhibitors (Table 2) (also see the Supporting information Figs. s1 and s2; Cornish Bowden Plots and s3-s41 for the IC_{50} plots for the inhibition of BuChE).

The most essential features for good BuChE inhibition are highlighted in Fig. 4 above.

MAO inhibition studies

As described above, besides being a target for Parkinson's disease, MAO is also a target for AD, and for this reason, considering the importance of the *N*-propargylamine pharmacophore, we developed a

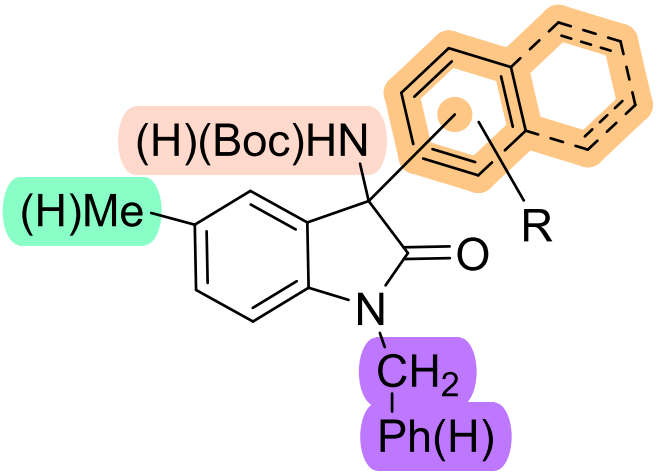

Fig. 4. Summarizes the most desirable features for good BuChE inhibition (both 1- and 2-naphthyl units provide excellent potencies).

series of *N*-propargyl-3-amino-3-aryl-oxindole analogues, **(10a-c)** and **(11a-d)** including, some Boc protected non-propargylated (**(5c)**), and free amine derivatives **(7c)**, **(7l)** and **(7m)** (Table 3). The best inhibition values were obtained against MAO-B using **(5c)** and **(11a)** (19.7% and 20.8% inhibition). Unfortunately, for the other derivatives, no relevant MAO inhibition was observed.

In silico studies

The possible binding of compounds to ChEs was investigated using in silico docking protocols using the X ray-determined protein crystal structures of human AChE and BuChE [23] ((Table 4). Nearly all of the compounds studied showed very strong predicted ligand binding efficiencies, within values determined previously [24,25].

Some of the results shown in Table 1, corroborated the results from the screening studies, for example; compound **(2c)** which furnished an IC_{50} of 0.29 μM (Table 1) gave a docking score of −9.82 kcal/mol and a glide ligand efficiency of −0.339. Compound **(5c)** which exhibited an IC_{50} of 27 nM (Table 1) gave a docking score of −8.02 kcal/mol and a glide ligand efficiency of −0.229 for the (*R*)-enantiomer. Both (*S*)- and (*R*)-**(4i)** gave scores of −9.72 and −10.54 kcal/mol (with ligand efficiencies of −0.324 and −0.351, respectively) when the IC_{50} of the racemate was determined to be 3.4 μM (Table 1). Also **(3i)** gave a value

Table 3
MAO screening data for selected 3-amino-aryl-oxindole analogues.

Compound[a]	Inhibition [%] at 1 μM ± SD[b]	
	MAO-A	**MAO-B**
5c	6.7 ± 4.3	19.7 ± 6.5
7c	10.3 ± 4.7	12.9 ± 8.3
7 l	6.8 ± 5.2	13.1 ± 11.4
7 *m*	6.4 ± 7.3	11.9 ± 11.2
10a	8.9 ± 3.6	9.8 ± 4.5
10b	11.1 ± 2.8	18.0 ± 11.6
10c	9.4 ± 3.4	18.3 ± 6.6
11a	9.1 ± 5.6	20.8 ± 12.3
11b	12.1 ± 11.6	17.6 ± 4.4
11c	9.4 ± 11.1	8.1 ± 4.8
11d	6.8 ± 1.8	11.9 ± 4.6
No inhibitor	0.0 ± 2.5	0.0 ± 3.8
Clorgyline	101.6 ± 1.3	31.4 ± 1.8
Safinamide	7.2 ± 3.4	96.9 ± 1.0

[a] Compounds dissolved in DMSO (10 mM, 1 mM).
[b] MAO-A and MAO-B inhibition were calculated as percentages related to control at a test concentration of 1 μM and given as mean ± standard deviation of two independent experiments in triplicate, using clorgyline and safinamide as a positive control.

Table 4
Calculated docking scores and efficiency indices for compounds with *h*BuChE.

Compound	Docking Score (kcal/mol)	Glide Ligand Efficiency	Glide Ligand Efficiency SA	Glide Ligand Efficiency Ln
***S*-(2a)**	−9.49	−0.365	−1.082	−2.229
***R*-(2a)**	−6.89	−0.265	−0.785	−1.618
***S*-(2b)**	−6.19	−0.238	−0.706	−1.454
***R*-(2b)**	−5.80	−0.223	−0.660	−1.361
***S*-(2c)**	−6.73	−0.232	−0.713	−1.540
***R*-(2c)**	−9.82	−0.339	−1.040	−2.248
***S*-(2d)**	−8.47	−0.292	−0.897	−1.938
***R*-(2d)**	−8.34	−0.288	−0.884	−1.910
***S*-(2e)**	−6.75	−0.241	−0.732	−1.558
***R*-(2e)**	−6.10	−0.218	−0.661	−1.408
***S*-(2f)**	−6.50	−0.241	−0.722	−1.513
***R*-(2f)**	−6.47	−0.240	−0.719	−1.505
***S*-(2 g)**	−6.35	−0.244	−0.723	−1.491
***R*-(2 g)**	−6.38	−0.245	−0.727	−1.498
***S*-(2 h)**	−8.66	−0.333	−0.987	−2.035
***R*-(2 h)**	−6.83	−0.263	−0.778	−1.603
***S*-(2i)**	−6.97	−0.268	−0.794	−1.636
***R*-(2i)**	−6.90	−0.265	−0.786	−1.619
***S*-(2j)**	−5.55	−0.205	−0.616	−1.291
***R*-(2j)**	−6.50	−0.241	−0.723	−1.514
***S*-(3a)**	−8.33	−0.278	−0.863	−1.893
***R*-(3a)**	−9.51	−0.317	−0.985	−2.160
***S*-(3b)**	−6.98	−0.258	−0.775	−1.624
***R*-(3b)**	−9.40	−0.348	−1.045	−2.189
***S*-(3c)**	−7.14	−0.275	−0.814	−1.677
***R*-(3c)**	−7.46	−0.287	−0.850	−1.751
***S*-(3d)**	−7.28	−0.270	−0.809	−1.694
***R*-(3d)**	−8.15	−0.302	−0.906	−1.898
***S*-(3e)**	−9.75	−0.325	−1.010	−2.216
***R*-(3e)**	−7.57	−0.252	−0.784	−1.720
***S*-(3f)**	−4.77	−0.170	−0.517	−1.101
***R*-(3f)**	−5.40	−0.193	−0.585	−1.245
***S*-(3 g)**	−6.21	−0.230	−0.690	−1.446
***R*-(3 g)**	−5.65	−0.209	−0.628	−1.316
***S*-(3 h)**	−7.47	−0.277	−0.830	−1.739
***R*-(3 h)**	−9.10	−0.337	−1.011	−2.119
***S*-(3i)**	−6.99	−0.259	−0.777	−1.628
***R*-(3i)**	−9.78	−0.362	−1.087	−2.278
***S*-(3 k)**	−4.38	−0.156	−0.475	−1.011
***R*-(3 k)**	−8.58	−0.307	−0.931	−1.982
***S*-(4a)**	−6.65	−0.237	−0.721	−1.535
***R*-(4a)**	−5.32	−0.190	−0.577	−1.229
***R*-(4a)**	−5.32	−0.190	−0.577	−1.229
***R*-(4b)**	−7.02	−0.260	−0.780	−1.634
***S*-(4c)**	−7.60	−0.253	−0.787	−1.726
***R*-(4c)**	−7.35	−0.245	−0.761	−1.670
***S*-(4d)**	−6.67	−0.256	−0.760	−1.566
***R*-(4d)**	−6.22	−0.239	−0.709	−1.461
***S*-(4e)**	−6.87	−0.245	−0.745	−1.585
R-(4e)	−6.12	−0.219	−0.664	−1.413
***S*-(4f)**	−6.81	−0.252	−0.756	−1.585
***R*-(4f)**	−7.02	−0.260	−0.780	−1.633
***S*-(4 g)**	−6.96	−0.240	−0.738	−1.594
***R*-(4 g)**	−7.37	−0.254	−0.780	−1.687
***S*-(4 h)**	−7.11	−0.263	−0.790	−1.654
***R*-(4 h)**	−6.32	−0.234	−0.702	−1.471
S-(4i)	−9.72	−0.324	−1.006	−2.207
***R*-(4i)**	−10.54	−0.351	−1.092	−2.395
***S*-(5c)**	−7.82	−0.223	−0.730	−1.716
***R*-(5c)**	−8.02	−0.229	−0.749	−1.760
***S*-(7c)**	−9.54	−0.341	−1.034	−2.201
***R*-(7c)**	−8.80	−0.314	−0.954	−2.030

Compounds with docking scores < -8.0 kcal/mol are shaded in light brown. Not all the compounds screened in silico were biologically assayed.

of 11.0 μM and a docking score of −9.78 kcal/mol for the (*R*)-enantiomer.

Since both enantiomers were screened, it was of interest to determine if one enantiomer was favored over the other. In the case of the **(2)** series, it was generally the (*S*) enantiomer that was preferred, however, in the case of the other series, there was no common trend.

It should also be noted, that gratifyingly there was a correlation between the IC_{50} values reported in the bioassay studies and these in silico docking results.

In the case of compounds **(5c)** and **(7c),** the simulations for both enantiopodes predicted good binding to the *h*BChE binding site through favourable π stacking of the oxindole ring with Trp82 (Fig. 5), in addition to π stacking with Trp231 and Phe329 in the case of (*R*)-**(5c)**, and His438 for (*S*)-**(7c)**. These are in addition to general van der Waals and polar interactions between the ligands and the protein, such as the hydrogen bond donated from Gly117 to the 3-carbonyl of the oxindole ring of (*S*)-**(7c)**.

Saturation transfer difference (STD)-NMR studies

Over the last years, the STD-NMR method has become an indispensable technique to validate docking studies (in silico) [13,14,22]. To gain better insight into the interactions of our 3-aminooxindoles with *eq*BuChE, we executed STD-NMR experiments with our most potent oxindole ligands, namely **(2c)** and **(5c)**. These STD-NMR studies showed why **(5c)** is a stronger inhibitor of *eq*BuChE than **(2c)**.

STD-NMR of ligand (2c). Upon analyzing the results obtained in the STD-NMR experiment of **(2c)** (Fig. 6) with *eq*BuChE, (the graph of the STD amplification factor as a function of saturation time is shown in the Supporting Information (Fig. s42)), it was observed that all the hydrogens interact with the *eq*BuChE binding pocket. Nevertheless, the H1 and H13 hydrogens from the methyl and *t*-butyl groups showed weaker interactions with the amino acid residues (with attenuations of 55% and 29%, respectively). In fact, these results are in agreement with the docking studies, in which the role of the *t*-butoxide group interacts weakly with the enzyme. As can be observed from the epitope intensity table shown in Fig. 6, the aromatic hydrogens are the most affected by the active site residues, having attenuations in the range 81–100%. This was indeed corroborated by the docking study (Fig. 5), showing very good placement of the aromatic units within the binding pocket.

STD-NMR of ligand (5c). The STD-NMR results for **(5c)** with *eq*BuChE are shown in Fig. 7 (the graph of the STD amplification factor as a function of saturation time is shown in Fig. s43; SI). The signals for the non-aromatic protons H2 and H7 showed a weaker interaction with the enzyme, which are completely in agreement with docking studies (Fig. 5). As can be seen from the epitope intensity table shown in Fig. 7, the aromatic protons are the most affected, with attenuations in the range 87–100%. This was in fact supported by the docking study (Fig. 5), showing good proximity of the Trp231 and Phe329 units to the phenyl ring of the benzyl group (97% attenuation). The oxindole hydrogens, H3-H6 showed high STD attenuation values (95.7 – 99.6%) indicating that they should be very close to the active site residues of the protein, and most probably to Trp82 as suggested by our docking studies (Fig. 5). The naphthyl protons also showed high proximity to the amino acid residues of the enzyme, showing high STD attenuation values, more specifically H10 and H11 with values of 100%. The docking studies indicated the proximity of these hydrogens to the polar amino acid residues of the enzyme.

On comparing the STD-NMR results for both inhibitors, we confirm that **(5c)** is a stronger binder than **(2c)**, which is principally due to the benzyl group which establishes a stronger interaction with aminoacid residues of the binding site, which is corroborated by our docking studies.

Calculated physicochemical properties

For some of the chosen compounds we determined their physicochemical properties, using SwissADME [26]. All of the calculated results were within the limits defined for Lipinski's rules, except in the case of **(5c)**, **(5d)**, and **(11b)**, which were slightly outside the defined limits. Also, encouragingly, none of these compounds were identified as Pan-

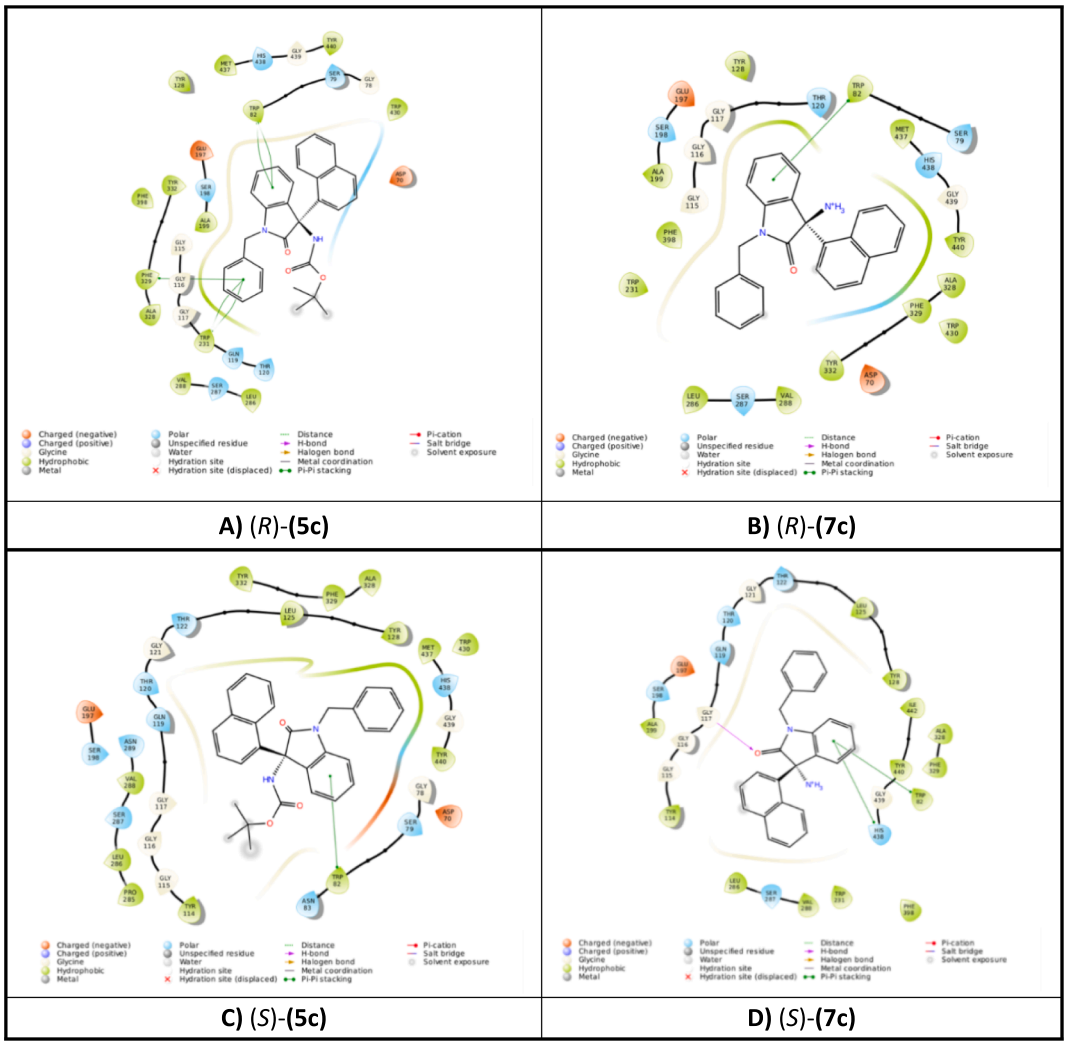

Fig. 5. 2D schematic representation of predicted binding poses in the binding site of *h*BuChE with: A) (*R*)-**(5c)**, B) (*R*)-**(7c)**, C) (*S*)-**(5c)**, *and* D) (*S*)-**(7c)**. Note: the protonated form of **(7c)** was considered.

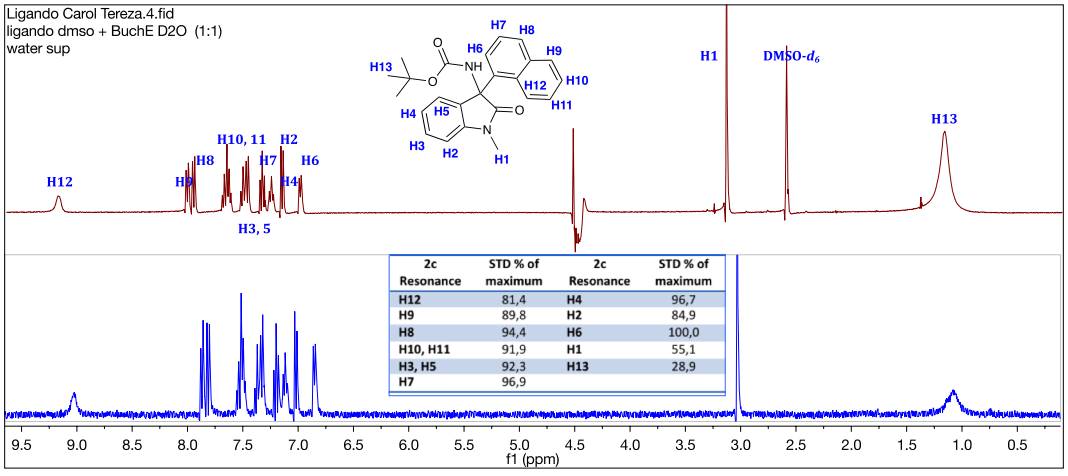

2c Resonance	STD % of maximum	2c Resonance	STD % of maximum
H12	81,4	H4	96,7
H9	89,8	H2	84,9
H8	94,4	H6	100,0
H10, H11	91,9	H1	55,1
H3, H5	92,3	H13	28,9
H7	96,9		

Fig. 6. Top: Reference ^{1}H NMR spectrum of compound **(2c)** (5.5 mM) with *eq*BuChE enzyme (1.3 μM). Bottom: the corresponding STD-NMR spectrum with 4 s of saturation. The H6 proton was set to 100%. The NMR spectra were recorded at 25 °C.

Assay Interference Compounds (PAINS) or in other words, suggesting no interactions with multiple targets with a possible negative influence on any screening experiment (Table 5). All the synthesized compounds were predicted to be amenable to gastrointestinal absorption, as well as predicted to cross the blood–brain barrier (BBB). Most of the products were predicted to be moderately soluble in water, and a few **(5b)**, **(5c)**,

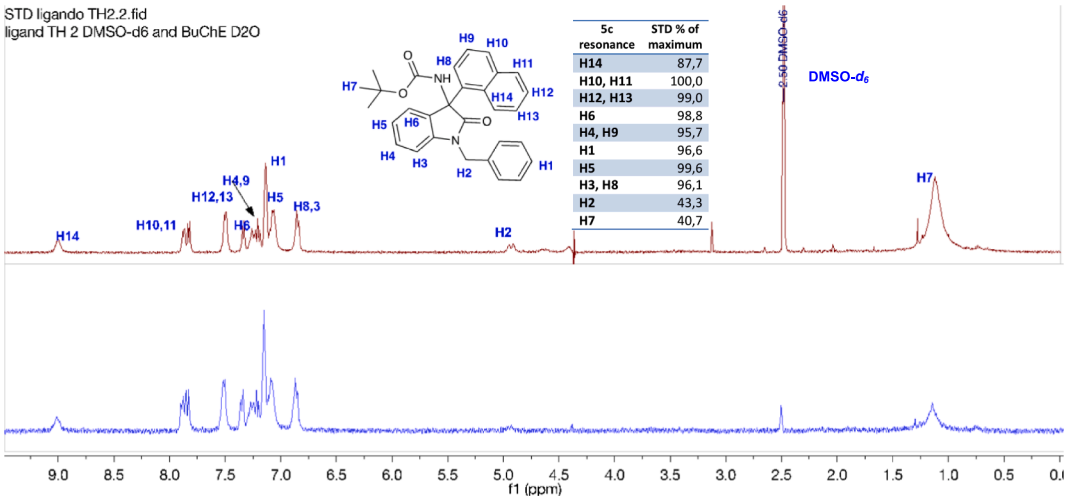

Fig. 7. TOP: Reference ^{1}H NMR spectrum of compound **(5c)** (2.3 mM) with *eq*BuChE enzyme (1.9 μM). Bottom: the corresponding STD-NMR spectrum with 4 s of saturation (bottom). The H3 proton was set to 100%. The NMR spectra were recorded at 25 °C.

Table 5
Calculated molecular properties for selected compounds.

Compound	Mw (g/mol)	MLOGP [28]	LogS [27]	# H-bond acceptors	# H-bond donors	TPSA	PAINS # alerts
(1d)	336.38	2.97	− 4.77	4	0	58.97	0
(2c)	388.46	3.32	− 5.47	3	1	58.64	0
(4c)	402.49	3.53	− 5.86	3	1	58.64	0
(4i)	402.49	3.53	− 5.86	3	1	58.64	0
(5a)	414.50	3.70	− 5.73	3	1	58.64	0
(5b)	428.52	3.90	− 6.11	3	1	58.64	0
(5c)	464.55	4.31	− 7.03	3	1	58.64	0
(5d)	448.94	4.17	− 6.38	3	1	58.64	0
(5e)	444.52	3.36	− 5.90	4	1	67.87	0
(5f)	432.49	4.07	− 5.84	4	1	58.64	0
(6a)	428.52	3.90	− 6.11	3	1	58.64	0
(6b)	442.55	4.10	− 6.49	3	1	58.64	0
(7j)	342.43	3.61	− 4.52	2	1	46.33	0
(7*n*)	367.24	3.37	− 4.23	2	1	46.33	0
(7o)	302.37	2.99	− 3.89	2	1	46.33	0
(10a)	429.51	3.23	− 4.61	3	1	61.88	0
(11a)	352.43	3.75	− 4.12	2	1	32.34	0
(11b)	402.49	4.38	− 5.42	2	1	32.34	0

MW = molecular weight; # H-bond = number of hydrogen bond; TPSA = topological surface area (Å^{2}).

(5d), **(6a)**, and **(6b)** poorly soluble [27,28] (Table 5).

Antiproliferative tests in SH-SY5Y human neuroblastoma cell line

The *in vitro* antiproliferative activity of the six most active compounds resulting from the BuChE tests (Table 1) was studied against the Alzheimer's disease model human neuroblastoma cell line, SH-SY5Y line using our implementation of the NCI protocol [29]. Thus, compounds **(2c)**, **(4c)**, **(4i)**, **(5c)**, **(7n)** and-**(7o)** were screened against the neuroblastoma cell line SH-SY5Y. This serves as a model for neurodegenerative disorders and is widely used in neurotoxicity studies [29]. The results of the 50% growth inhibition values after 48 h of exposure (GI_{50}) are given in Table 6. The results show that compounds **(5c)**, **(7n)** and **(7o)** were inactive ($GI_{50} > 100$ μM) against this neuroblastoma cell-line. In contrast, compounds **(2c)**, **(4c)** and **(4i)** were cytotoxic, with GI_{50} values in the range 19–46 μM.

Label-free continuous live cell imaging

Live imaging enables one to observe cytostatic effects [30] or cell death of treated cells in real time and to identify several apoptotic hallmarks [32–35]. For characterization of the phenotypic effects of BuChE inhibitors on neuroblastoma cells, the evolution of the culture was monitored every 5 min using label-free holotomographic 3D microscopy. SH-SY5Y cells were exposed to compounds **(2c)**, **(5c)** and **(7o)** for 20 h at 100 μM (Supplementary material, videos S1–4). The selection was done considering the BuChE tests (Table 1) and the antiproliferative activity against this neuroblastoma cell line (Table 6). Untreated and treated cells moved freely and divided, indicating that the exposure to the compounds apparently did not affect cell growth and motility. A more precise analysis after segmentation of the single cells

Table 6
Antiproliferative activity (GI_{50}) against the SH-SY5Y human neuroblastoma cell line.[a]

Compound	SH-SY5Y Cell line GI_{50} values
(2c)	37 ± 7.0
(4c)	19 ± 5.2
(4i)	21 ± 5.1
(5c)	>100
(7n)	>100
(o)	>100
CDDP	14 ± 2.4

[a] GI_{50} values are given in μM. Standard deviation was calculated from two to four independent experiments. Cisplatin (CDDP) was used as a reference cytotoxic drug.

over the images of the 240 cycles inferred from the refractive index (RI) measurements for each individual cell provided phenotypic-related parameters at each time point. Thus, the normalized cell count (Fig. 8A) showed slight antiproliferative effects only for compound **(2c)**, consistent with the GI_{50} values reported in Table 6. When considering the compactness (Fig. 8B), compound **(7o)** was the one that affected most the morphology of SH-SY5Y cells. In neurons, cell compactness is an indicator of the presence of multiple neurites. The higher values, the more neurites, whilst a value of 1 indicates that the cell is circular, i.e., no neurites. Another relevant morphological parameter for neurons is cell extent. Extent is a measure of the cell's ability to spread out. A value close to 0 indicates spreading, whilst values close to 1 match with a circular or a line shape. In the particular case of neurons, an extent value of 1 occurs in neurons with a log axon, while neurons with many radiating axons in all directions provide an extent value of 0. Fig. 8C shows that all tested compounds induce larger extent values when compared to untreated cells. The change in extent values for treated cells at short exposure times indicates a rapid absorption of the compound by the cells. As a measurement of cell damage, granularity is a parameter that reflects the state of organelle organization, and as such, allows to track changes in cell content. As observed in Fig. 8D, the compounds did not affect internal cell organization. Overall, continuous live imaging experiments point out that the compounds under study do not induce relevant cell damage and thus, the compounds might be interesting drug candidates against Alzheimer's disease.

DPPH antioxidant assays

The antioxidant properties of the six selected compounds **(2c), (4c), (4i), (5c), (7n)** and **(7o)** as well as galantamine were evaluated using the 2,2-diphenyl-1-picrylhydrazyl (DPPH) radical scavenging assay, which is a well-established method for determine the antioxidant activity (Table 7). In this method the antioxidants react with DPPH, and convert it to yellow-colored diphenylpicrylhydrazine [35]. The selected compounds and galantamine were evaluated in the range of concentrations between 0.75 and 100 μM. The compounds and galantamine didn't show antioxidant activity in the concentration range studied. Ascorbic acid was used as a positive control in this assay, and showed 82% of inhibition at 50 μM.

Table 7
Results of DPPH Inhibition (%).

Compound (concentration μM)	% Inhibition of DPPH
(2c) (100)	4
(4c) (100)	5.5
(4i) (100)	5
(5c) (100)	3
(7n) (100)	7.5
(7o) (100)	6
Galantamine (50)	5
Ascorbic Acid (50)	82

Conclusions

This work is a continuation of our previous work on the catalytic arylation of isatin-derived *N*-Boc ketimines providing chiral 3-aryl-3-amino-2-oxindoles. The difference is that a series of *N*-benzyl analogues were synthesized, and a group of novel *N*-propargyl analogues were prepared. These compounds were screened in various bioassays; against AChE, BuChE and MAO (MAO-A and B). They were found to be selective and very potent inhibitors of BuChE. For example, many showed potencies of lower than 1 μM level and in fact **(5c)** showed a 27 nM activity, which far exceeded the potency of the drug galantamine, used as a positive control. The *N*-propargyl analogues were only moderately active against both MAO-A and B (best result 20% inhibition for MAO-B and 13% for MAO-A). The compounds that were tested for anti-oxidation activity were shown to be inactive, and *in vivo* screening in the human neuroblastoma cell line SH-SY5Y showed that some of the tested compounds were non-cytotoxic and others mildly cytotoxic, although real time cell imaging studies showed that the compounds did not induce cell damage, and might be good candidates for Alzheimer's disease treatment.

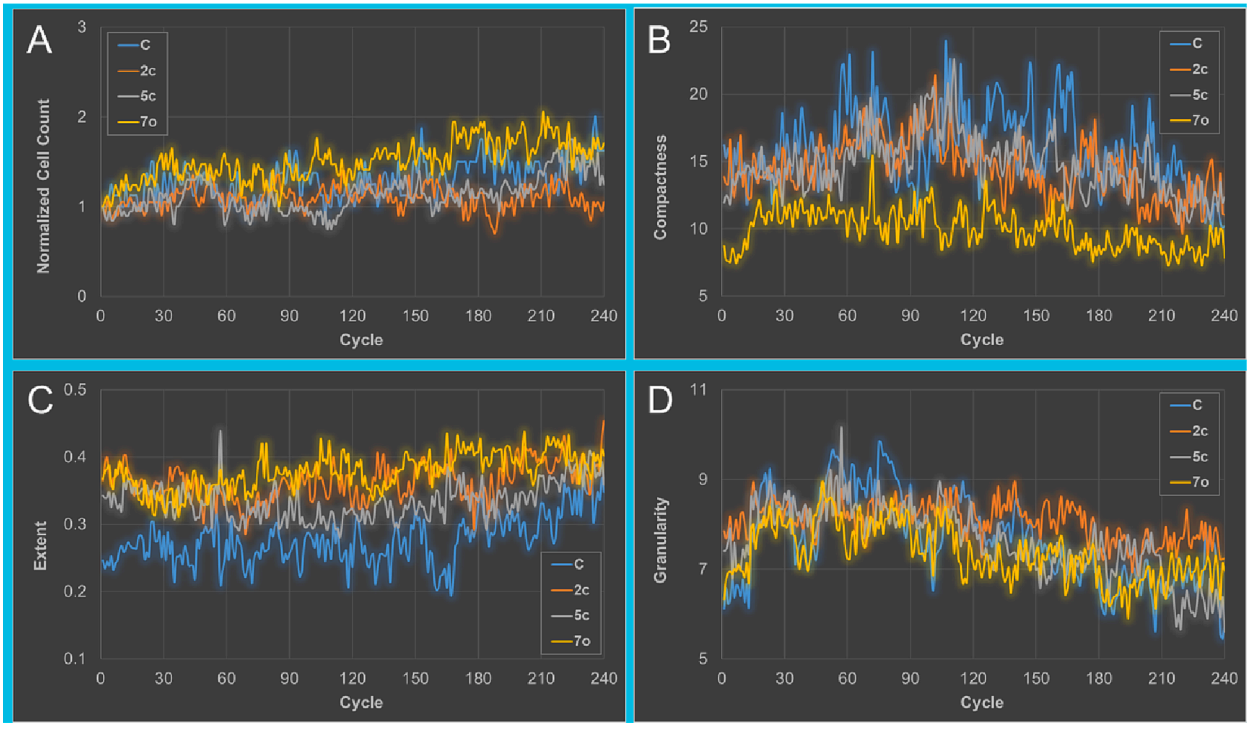

Fig. 8. Kinetics for untreated SH-SY5Y cells, and cells exposed to compounds **(2c)**, **(5c)** and **(7o)** at 100 μM for 20 h.

Experimental section

General considerations

Reagents were obtained from Sigma Aldrich, Acros, Strem, and Alfa Aesar and were used as received. The solvents used were dried using standard laboratory techniques [37]. Reactions were conducted in a Radley's® 12-position carousel reactor or in round-bottomed flasks, under a nitrogen atmosphere. Column chromatography was carried out on silica gel (Carlo Erba, 40–63 μm (flash) and 60–200 μm, 60 Å). Thin-layer chromatography (TLC) was carried out on aluminum-backed Kieselgel 60 F254 plates (Merck and Machery Nagel). Plates were visualized either by UV light or with phosphomolybdic acid in ethanol. Melting points (m.p.) were determined with a Barnstead Electrothermal 9100 apparatus and are uncorrected. NMR spectra were recorded with a Bruker Avance III instrument (400 MHz) with a broadband probe. Chemical shifts are quoted in parts per million (ppm) relative to 0.0 ppm and were referenced to the appropriate non-deuterated solvent peak. Coupling constants (*J*) are reported in Hz and refer to apparent peak multiplicities. Splitting patterns are reported as s, singlet; d, doublet; dd, double of doublets, t, triplet; m, multiplet; br, broad. HR-MS Analysis was performed on a Thermo Orbitrap Q-exactive focus on a resolution of 70,000 at the Chemistry Department, University of Salamanca (by Dr. César Raposo). ESI was used as an ionization method, and an alternating method between positive and negative modes was applied. The one with the best signal was used for the determination of the exact mass. Samples were dissolved in methanol.

Full characterization of compounds **(1a-c)**, **(2a-k)**, **(3a-k)**, **(4a-i),** and **(7 l)** can be found in the literature [20], as well as the *N*-benzyl isatin derivatives **(5a)-(5 h)**, **(6a)-(6c), (7a)**, **(7i)**, **(7j)**, **(7 m)**, **(7n)** and **(7o)** [21].

General conditions to access isatin-derived n-Boc-protected ketimines (1d-e) [20]

To a stirred solution of *tert*-butyl (trimethylsilyl)carbamate (4.21 mmol) in THF (8 ml), butyllithium (1 eq) was added at −78 °C. After stirring for 1 h, *N*-benzyl isatin or its derivatives (1 eq) in THF (8 ml) was added dropwise. The reaction mixture was allowed to stir for an additional 5 h. Then the trimethylsilyl chloride (1.1 eq) was slowly added to the mixture. During the next 2 h, the reaction was warmed up to room temperature followed by mixing with aqueous $NaHCO_3$ and extraction with ethyl acetate. The combined organic layers were dried by anhydrous $MgSO_4$ and concentrated under reduced pressure. The crude mixture was purified by column chromatography on silica gel using a mixture of hexane/Et_2O (5/1) and (1/1) as eluents furnishing the desired compounds.

General procedure for the Rh-Catalysed addition of arylboronic acids to ketimines [20]

In a Radley's® 12 position carousel reactor under a nitrogen atmosphere the $Rh(COD)BF_4$ (3 mol%), ketimine or its derivatives **(1d-e)**, $ArB(OH)_2$ (2 eq), NEt_3 (2 eq), and toluene (1.5 ml) were added. The reaction was left stirring at 60 °C for 24 h. After that, the solvent was evaporated followed by purification of the crude product by column chromatography on silica gel using a mixture of hexane/Et_2O (3/1) and (1/1) as eluents, delivered the desired compounds **(5a-h) and (6a-c)**.

General conditions for deprotection of the Boc group

3-*N*-Boc-3-aryl-2-oxindole (**(2)**, **(3)**, **(4)**, **(5)** or **(6)**), 1 eq) and CH_2Cl_2 were added to a round-bottomed flask. The mixture was cooled down to 0 °C and the TFA (3.8 eq) was added to the solution. It was left stirring at 0 °C for 2 h and monitored with TLC. The reaction mixture was concentrated under reduced pressure followed by purification of the crude mixture by column chromatography on silica gel using a mixture of hexane/Et_2O (3/1) and (1/1) as eluents. If the desired compound is still impure, the following procedure (protonation) was followed: the compound was dissolved in 1 ml of EtOH. Then, 5–10 drops of concentrated HCl were added and the mixture was allowed to stir for 15 min. The solvent was evaporated and the solid recrystallized with EtOAc. The solid collected was dried under reduced pressure to afford the desired 3-amine-aryl-oxindole derivatives (**7**).

Biological evaluation

ChE inhibition assays

Measuring the anticholinesterase activity of compounds prepared herein was accomplished using acetylcholinesterase (AChE) from *Electrophorus electricus* (Type V-S), and butyrylcholinesterase (BuChE) (equine serum) as model enzymes (Sigma-Aldrich).

Minor modifications from the original Ellman assay [22,38] were used; assays were carried out at 25 °C in a buffered medium (pH 8.0, phosphate buffer) with acetylthiocholine and butyrylthiocholine as model substrates.

Monitoring of the enzymatic activity, in the absence and the presence of inhibitors, was conducted in a Thermo Scientific™ Varioskan™ LUX microplate reader, with Greiner F-bottom 96-well plates. The first screening was carried out at a 50 μM inhibitor concentration, keeping $[S] = K_M$. For those compounds showing %I > 50% at such concentration, IC_{50} values were obtained by plotting %I *vs.* log[I].

Cornish-Bowden plots (1/V *vs.* [I] and [S]/V *vs.* [I]) were used for the visualization of the mode of inhibition of the most active compounds. Calculation of the kinetic parameters (K_M, V_{max}) was accomplished using a nonlinear regression analysis (least squares fit) implemented in GraphPad Prism 8.01 software. The following equations were used for calculating the inhibition constants of the mixed inhibitors obtained herein:

$$K_{m,app} = K_M \frac{1 + \frac{[I]}{K_{ia}}}{1 + \frac{[I]}{K_{ib}}}$$

$$V_{max,app} = \frac{V_{max}}{1 + \frac{[I]}{K_{ia}}}$$

K_{ia}: Inhibition constant for the interaction of the inhibitor with the free enzyme (E).

K_{ib}: Inhibition constant for the interaction of the inhibitor with the complex enzyme-substrate (E-S).

MAO

A discontinuous fluorimetric assay of monoamine oxidases was conducted for both MAO-A and B isoforms as described previously [39]. One-point screening of the compounds was performed in duplicate in at least three independent experiments.

Kynuramine was used as a substrate for membrane-bound MAO-A and MAO-B (Sigma-Aldrich, MO, USA) at two-fold K_M concentration (K_M = 30 μM for MAO-A and K_M = 20 μM for MAO-B). The mixture in a total volume of 100 μL was pipetted onto flat-bottomed black 96-well plates (No. 655076, Greiner bio-one GmbH, Austria). This procedure was partially automated using an EVO freedom pipetting robot (Tecan Trading AG, Switzerland). After 20 min of incubation, the enzyme reaction was stopped (37 °C) by the addition of 35 μL sodium hydroxide (2 N). The remaining enzyme activity was determined by the detection of 4-hydroxyquinoline (λ_{Ex} = 320 nm, λ_{Em} = 405 nm) using an infinite M1000 Pro microplate reader (Tecan Trading AG, Switzerland). Product formation in the absence of an inhibitor was used as a control to calculate the percentage of inhibition at a test concentration of 1 μM. At least three independent experiments were performed in duplicate and reported as mean ± standard deviation (%) using clorgyline and safinamide as references.

In silico studies

Protein X-ray crystal structures were obtained from the Protein Data Bank [https://www.rcsb.org/], 640w for AChE and 4aqd for BChE. All protein structures were determined at high resolution. The structures were inspected and assessed as adequate for docking, with resolutions of 2.35 Å and 2.5 Å, respectively. Hydrogen atoms were added with Maestro software [Schrödinger, 2020]. Docking was then performed by extra precision Glide XP [Schrödinger, 2020] with extended sampling, and the OPLS3e forcefield [40]. Physicochemical properties for the compounds were calculated with SwissADME [26].

STD- NMR spectroscopy experiment

The *eq*BuChE enzyme used in the STD-NMR experiments was from equine serum (lyophilized powder with phosphate buffer salts, ≥10 units/mg protein), and was purchased from Sigma-Aldrich. The STD-NMR spectroscopy experiments were performed on a Bruker Avance III 400 MHz HD spectrometer equipped with a 5 mm broadband (PABBO BB/19F-1H/D Z-GRD) resonance probe head. STD-NMR experiments were carried out with solvent suppression and a 10 ms spin-lock filter after the 90° pulse to reduce residual signals from the protein. For selective saturation, cascades of Gaussian pulses with a length of 50 ms and 40–60 dB of attenuation were employed, with an interpulse delay of 1 ms [41,42]. The on-resonance and off-resonance frequencies were set to 0 and 12000 Hz, respectively. STD-NMR controls were performed using the ligand itself. Blank experiments were performed to guarantee the absence of direct saturation of the ligand proton signals. The relaxation delay was properly adjusted so that the experiment time length was kept constant at 6.5 s. Water suppression at 1880 Hz (4.7 ppm) was conducted. A sweep-width of 8012.82 Hz (20.03 ppm) was employed. The saturation times to obtain the STD epitope mapping were recorded at 0.25, 0.5, 1, 2, 3, 4, and 5 s [41,42]. STD spectrum was obtained by subtraction of saturated spectrum from the reference spectrum. STD intensity of individual signal was measured relative to the corresponding signal intensity in the reference spectrum. A stock solution of compound **(2c)** (ligand) was prepared in DMSO-d_6 with 11 mM of concentration. The stock solution of *eq*BuChE was prepared in D_2O with 2.5 μM of concentration. The sample for STD-NMR analysis was prepared by adding 300 μL of the solution stock of compound **(2c)** to a 300 μL of *eq*BuChE enzyme solution. A stock solution of compound **(5c)** (ligand) was prepared in DMSO-d_6 with 6 mM of concentration. The stock solution of *eq*BuChE was prepared in D_2O with 5 μM of concentration. The sample for STD-NMR analysis was prepared by adding 500 μL of the solution stock of compound **(5c)** to a 300 μL of *eq*BuChE enzyme solution.

Cell lines and culture

Cells were grown in RPMI-1640 medium containing 5% fetal bovine serum (FBS), 2 mM L-glutamine, 100 U/mL of penicillin G and 0.1 mg/mL of streptomycin in a 37 °C, at a 95% humidified atmosphere of 5% CO_2. Cells were maintained in culture in 60 mm cell culture dishes in growth medium (10 ml) and weighed twice a week.

Cell morphology

CX-A imaging platform microscope (Nanolive SA, Lausanne, Switzerland) was used to measure refractive indices, creating a holotomographic 3D image of the cells. SH-SY5Y cells were seeded onto 35 mm cell culture imaging dishes (ibidi GmbH, Gräfelfing, Germany) at a density of 50.000 cells/well. On the next day, cells were exposed to the test compound right before the acquisition of the images. Image data was transferred to FIJI software (NIH, USA) for image analysis. EVE software (Nanolive S.A.) was used for the analysis of the refractive indices and calculation of the average dry mass density.

DPPH antioxidant assay

Method adapted from a previously described procedure [36] Compounds **(2c)**, **(4c)**, **(4i)**, **(5c)**, **(7n)**, **(7o)** and galantamine (30 μL) at the desired concentration (0.75–100 μM) in methanol were added to a 96-well plate, followed by the addition of a solution of 2,2-diphenyl-1-picrylhydrazyl (DPPH) in methanol (200 μL, 100 μM). The final solution was incubated during 30 min in the dark. Then the absorbances of the DPPH in 30 μL of methanol and DPPH (200 μL (the blank) and the compounds plus DPPH in methanol were measured at 517 nm using a Microplate Spectrophotometry (TriStar® S LB 942 model instrument) in triplicate. Ascorbic acid was used as the positive control. Results are expressed as a percentage of DPPH inhibition according to the following formula:

$$\%\text{DPPH inhibition} = [(\text{Absblank} - \text{Abssample})/\text{Absblank})]\text{x}100$$

the words; blank and sample, should be subscripted.

Declaration of Competing Interest

The authors declare that they have no known competing financial interests or personal relationships that could have appeared to influence the work reported in this paper.

Data availability

Data will be made available on request.

Acknowledgments

We acknowledge the Fundação para a Ciência e a Tecnologia (FCT) for funding through the strategic project to LAQV-REQUIMTE (FCT/MCTES; UIDB/50006/2020|UIDP/50006/2020). O.L. and J.G.F.-B. thank Grant PID2020-116460RB-I00 funded by MCIN/AEI/10.13039/501100011033 and Junta de Andalucía (FQM-134) for financial support. A.T.G.-S. thanks to the Estonian Research Council (PRG1509) for funding. A.G.-B., A.P. and J.M.P. thank the Spanish Government (Project PID2021-123059OB-I00 funded by MCIN/AEI /10.13039/501100011033 / FEDER, UE). A.P. thanks the EU Social Fund (FSE) and the Canary Islands ACIISI for a predoctoral grant TESIS2020010055. A. G.-B. thanks the Asociación Española Contra el Cáncer (AECC) for a predoctoral grant. We are extremely grateful to COST Action 15135, a Multi-target paradigm for innovative ligand identification in the drug discovery process (MuTaLig). Also, TH thanks both the University of Hradec Králové (Faculty of Science) and the Erasmus + program for a travel grant (2019-1-CZ01-KA103-060058).

Appendix A. Supplementary data

Supplementary data to this article can be found online at https://doi.org/10.1016/j.rechem.2023.101032.

References

[1] S. Srivastava, R. Ahmad, S.K. Khare, Alzheimer's disease and its treatment by different approaches: a review, Eur. J. Med. Chem. 216 (2021), 113320, https://doi.org/10.1016/j.ejmech.2021.113320.

[2] Shi En Kim FDA to review another Alzheimer's antibody Chemical & Engineering News 100 25 2022 12 12.

[3] H. Devlin H.D.S. correspondent, Success of experimental Alzheimer's drug hailed as 'historic moment' The Guardian. 2022 accessed October 31, 2022). A. King, Biogen-Eisai's second Alzheimer's antibody approved in the US, ChemistryWorld, 20 (2023) 18. Second Alzheimer's antibody approved in the US | Business | Chemistry World https://www.theguardian.com/society/2022/sep/28/alzheimers-disease-progression-slowed-by-new-drug-lecanemab.

[4] B. Downer, S. Al Snih, L.-N. Chou, Y.-F. Kuo, M. Raji, K.S. Markides, K. J. Ottenbacher, A.B. Newman, Changes in health care use by mexican american medicare beneficiaries before and after a diagnosis of dementia, J. Gerontol.: Ser. A 76 (3) (2021) 534–542.

[5] Y.M. Khetmalis, M. Shivani, S. Murugesan, K.V.G. Chandra Sekhar, Oxindole and its derivatives: A review on recent progress in biological activities, Biomed. Pharmacother. 141 (2021), 111842, https://doi.org/10.1016/j.biopha.2021.111842.
[6] R. Xu, M. Zhan, L. Peng, X. Pang, J. Yang, T. Zhang, H. Jiang, L. Zhao, Y. Chen, Design, synthesis and biological evaluation of deuterated nintedanib for improving pharmacokinetic properties: Deuterated nintedanib, improving pharmacokinetic properties, J. Lab. Comp. Radiopharm. 58 (2015) 308–312, https://doi.org/10.1002/jlcr.3299.
[7] R. Roskoski, Sunitinib: A VEGF and PDGF receptor protein kinase and angiogenesis inhibitor, Biochem. Biophys. Res. Commun. 356 (2) (2007) 323–328.
[8] C.-S.-L. Gal, D. Raufaste, S. Derick, J. Blankenstein, J. Allen, B. Pouzet, M. Pascal, J. Wagnon, M.A. Ventura, Biological characterization of rodent and human vasopressin V $_{1b}$ receptors using SSR-149415, a nonpeptide V $_{1b}$ receptor ligand, American Journal of Physiology-Regulatory, Integ. Comp. Phys. 293 (2007) R938–R949, https://doi.org/10.1152/ajpregu.00062.2007.
[9] M. Rottmann, C. McNamara, B.K.S. Yeung, M.C.S. Lee, B. Zou, B. Russell, P. Seitz, D.M. Plouffe, N.V. Dharia, J. Tan, S.B. Cohen, K.R. Spencer, G.E. González-Páez, S. B. Lakshminarayana, A. Goh, R. Suwanarusk, T. Jegla, E.K. Schmitt, H.-P. Beck, R. Brun, F. Nosten, L. Renia, V. Dartois, T.H. Keller, D.A. Fidock, E.A. Winzeler, T. T. Diagana, Spiroindolones, a Potent Compound Class for the Treatment of Malaria, Science 329 (2010) 1175–1180, https://doi.org/10.1126/science.1193225.
[10] S.R.S. Rudrangi, V.K. Bontha, V.R. Manda, S. Bethi, Oxindoles and Their Pharmaceutical Significance- an Overview, Asian J. Res. Chem. 4 (2011) 335–338.
[11] M.A. Ali, R. Ismail, T.S. Choon, Y.K. Yoon, A.C. Wei, S. Pandian, R.S. Kumar, H. Osman, E. Manogaran, Substituted spiro [2.3′] oxindolespiro [3.2{\Prime}]-5,6-dimethoxy-indane-1{\Prime}-one-pyrrolidine analogue as inhibitors of acetylcholinesterase, Bioorg. Med. Chem. Lett. 20 (2010) 7064–7066, https://doi.org/10.1016/j.bmcl.2010.09.108. See for example:.
[12] J. Totobenazara, P. Bacalhau, A.A.S. Juan, C.S. Marques, L. Fernandes, A. Goth, A. T. Caldeira, R. Martins, A.J. Burke, Design, Synthesis and Bioassays of 3-Substituted-3-Hydroxyoxindoles for Cholinesterase Inhibition, ChemistrySelect 1 (2016) 3580–3588, https://doi.org/10.1002/slct.201600932.
[13] C.S. Marques, Ó. López, D. Bagetta, E.P. Carreiro, S. Petralla, M. Bartolini, M. Hoffmann, S. Alcaro, B. Monti, M.L. Bolognesi, M. Decker, J.G. Fernández-Bolaños, A.J. Burke, N-1,2,3-triazole-isatin derivatives for cholinesterase and β-amyloid aggregation inhibition: A comprehensive bioassay study, Bioorg. Chem. 98 (2020), 103753, https://doi.org/10.1016/j.bioorg.2020.103753.
[14] P. Bacalhau, L. Fernandes, M. Rosário Martins, F. Candeias, E.P. Carreiro, Ó. López, A. Teresa Caldeira, J. Totobenazara, R.C. Guedes, A.J. Burke, In silico, NMR and pharmacological evaluation of an hydroxyoxindole cholinesterase inhibitor, Bioorg. Med. Chem. 27 (2019) 354–363, https://doi.org/10.1016/j.bmc.2018.12.007.
[15] A. Almansour, R. Kumar, N. Arumugam, A. Basiri, Y. Kia, M. Ali, M. Farooq, V. Murugaiyah, A Facile Ionic Liquid Promoted Synthesis, Cholinesterase Inhibitory Activity and Molecular Modeling Study of Novel Highly Functionalized Spiropyrrolidines, Molecules 20 (2015) 2296–2309.
[16] A.M. Srour, D.H. Dawood, M.N.A. Khalil, Z.M. Nofal, Synthesis and 2D-QSAR study of dispiropyrrolodinyl-oxindole based alkaloids as cholinesterase inhibitors, Bioorg. Chem. 83 (2019) 226–234, https://doi.org/10.1016/j.bioorg.2018.10.030.
[17] P. Brandão, Ó. López, L. Leitzbach, H. Stark, J.G. Fernández-Bolaños, A.J. Burke, M. Pineiro, Ugi Reaction Synthesis of Oxindole−Lactam Hybrids as Selective Butyrylcholinesterase Inhibitors, ACS Med. Chem. Lett. 12 (2021) 1718–1725.
[18] S. Carradori, R. Silvestri, R, Silvestri, New Frontiers in Selective Human MAO-B Inhibitors, J. Med. Chem. 58 (17) (2015) 6717–6732.
[19] C. Binda, F. Hubalek, M. Li, Y. Herzig, J. Sterling, D.E. Edmondson, A. Mattevi, Crystal structures of monoamine oxidase B in complex with four inhibitors of the N-propargylaminoindan class, J. Med. Chem. 47 (2004) 1767–1774.
[20] C.S. Marques, A.J. Burke, Modular Catalytic Synthesis of 3-Amino-3-aryl-2-oxindoles: Rh Catalysis with Isatin-Derived *N*-Boc-Protected Ketimines, Eur. J. Org. Chem. 2016 (4) (2016) 806–812.
[21] C.S. Marques, Ó. López, L. Leitzbach, J.G. Fernández-Bolaños, H. Stark, A.J. Burke, Survey of New, Small-Molecule Isatin-Based Oxindole Hybrids as Multi-Targeted Drugs for the Treatment of Alzheimer's Disease, Synth. 54 (2022) 4304–4319, https://doi.org/10.1055/s-0041-1737343.
[22] A. Moutayakine, C. Marques, Ó. López, D. Bagetta, L. Leitzbach, S. Hagenow, E. P. Carreiro, H. Stark, S. Alcaro, J.G. Fernández-Bolaños, A.J. Burke, Evaluation of chromane derivatives: Promising privileged scaffolds for lead discovery within Alzheimer's disease, Bioorg. Med. Chem. 68 (2022), 116807, https://doi.org/10.1016/j.bmc.2022.116807.
[23] C. Hetényi, U. Maran, A.T. García-Sosa, M. Karelson, Structure-based calculation of drug efficiency indices, Bioinformatics 23 (2007) 2678–2685.
[24] A.T. García-Sosa, S. Sild, U. Maran, Docking and virtual screening using distributed grid technology, QSAR Combin. Sci. 28 (2009) 815–821, https://doi.org/10.1002/qsar.200810174.
[25] A.T. Garcia-Sosa, U. Maran, C. Hetenyi, Molecular Property Filters Describing Pharmacokinetics and Drug Binding 19 (2012) 1646–1662, https://doi.org/10.2174/092986712799945021.
[26] A. Daina, O. Michielin, V. Zoete, SwissADME: a free web tool to evaluate pharmacokinetics, drug-likeness and medicinal chemistry friendliness of small molecules, Sci. Rep. 7 (2017) 42717, https://doi.org/10.1038/srep42717.
[27] J. Ali, P. Camilleri, M.B. Brown, A.J. Hutt, S.B. Kirton, *In Silico* prediction of aqueous solubility using simple qspr models: the importance of phenol and phenol-like moieties, J. Chem. Inf. Modeling 52 (2012) 2950–2957, https://doi.org/10.1021/ci300447c.
[28] C.A. Lipinski, F. Lombardo, B.W. Dominy, P.J. Feeney, Experimental and computational approaches to estimate solubility and permeability in drug discovery and development settings, Adv. Drug Deliv. Rev. 46 (2001) 3–26, https://doi.org/10.1016/S0169-409X(96)00423-1.
[29] A. Puerta, A.R. Galán, R. Abdilla, K. Demanuele, M.X. Fernandes, G. Bosica, J. M. Padrón, Naphthol-derived Betti bases as potential SLC6A14 blockers, J. Mol. Clin. Med. 2 (2019) 35–40, https://doi.org/10.31083/j.jmcm.2019.02.7181.
[30] L.F. Hoffmann, A. Martins, F. Majolo, V. Contini, S. Laufer, M.I. Goettert, Neural regeneration research model to be explored: SH-SY5Y human neuroblastoma cells, Neural Regener. Res. 18 (2023) 1265–1266, https://doi.org/10.4103/1673-5374.358621.
[32] M.C. Padilla-Pérez, E.M. Sánchez-Fernández, A. González-Bakker, A. Puerta, J. M. Padrón, F. Martín-Loro, A.I. Arroba, J.M. García Fernández, C.O. Mellet, Fluoro-labelled sp2-iminoglycolipids with immunomodulatory properties, Eur. J. Med. Chem. 255 (2023), https://doi.org/10.1016/j.ejmech.2023.115390.
[33] R.E. Barrientos, E. Ibáñez, A. Puerta, J.M. Padrón, A. Paredes, F. Cifuentes, J. Romero-Parra, J. Palacios, J. Bórquez, M.J. Simirgiotis, Phenolic fingerprinting and bioactivity profiling of extracts and isolated compounds from *Gypothamnium pinifolium* Phil, Antioxid. 11 (2022) 2313, https://doi.org/10.3390/antiox11122313.
[34] R. Lacret, A. Puerta, S. Granica, A. González-Bakker, D. Hevia, Y. Teng, C. C. Sánchez-Mateo, P.L. Pérez de Paz, J.M. Padrón, Bioactive potential: a pharmacognostic definition through the screening of four hypericum species from the canary islands, Molecules 27 (2022) 6101, https://doi.org/10.3390/molecules27186101.
[35] A. Puerta, A. González-Bakker, G. Santos, J.M. Padrón, Early pharmacological profiling of antiproliferative compounds by live cell imaging, Molecules 27 (2022) 5261, https://doi.org/10.3390/molecules27165261.
[36] P. Michalska, P. Mayo, C. Fernández-Mendívil, G. Tenti, P. Duarte, I. Buendia, M. T. Ramos, M.G. López, J.C. Menéndez, R. León, Antioxidant, anti-inflammatory and neuroprotective profiles of novel 1,4-dihydropyridine derivatives for the treatment of alzheimer's disease, Antioxidants 9 (2020) 650, https://doi.org/10.3390/antiox9080650].
[37] W.L.F. Armarego, W.L.F. Armarego, D.D. Perrin, Purification of laboratory chemicals, 4 ed., Butterworth-Heinemann, Oxford, 2002.
[38] G.L. Ellman, K.D. Courtney, V. Andres, R.M. Featherstone, A new and rapid colorimetric determination of acetylcholinesterase activity, Biochem. Pharmacol. 7 (2) (1961) 88–95.
[39] A. Affini, S. Hagenow, A. Zivkovic, J. Marco-Contelles, H. Stark, Novel indanone derivatives as MAO B/H3R dual-targeting ligands for treatment of Parkinson's disease, Eur. J. Med. Chem. 148 (2018) 487–497, https://doi.org/10.1016/j.ejmech.2018.02.015.
[40] K. Roos, C. Wu, W. Damm, M. Reboul, J.M. Stevenson, C. Lu, M.K. Dahlgren, S. Mondal, W. Chen, L. Wang, R. Abel, R.A. Friesner, E.D. Harder, OPLS3e: extending force field coverage for drug-like small molecules, J. Chem. Theory Comput. 15 (2019) 1863–1874, https://doi.org/10.1021/acs.jctc.8b01026.
[41] S. Berger, S. Braun, 200 and More NMR Experiments - A Practical Course, (**2014**), Wiley-VCH.
[42] T.D.W. Claridge, High-Resolution NMR Techniques in Organic Chemistry, 3rd Edition, Elsevier, Oxford, 2016.

Further reading

[31] J.M. Roldán-Peña, A. Puerta, J. Dinić, S. Jovanović Stojanov, A. González-Bakker, F.J. Hicke, A. Mishra, A. Piyasaengthong, I. Maya, J.W. Walton, M. Pešić, J. M. Padrón, J.G. Fernández-Bolaños, Ó. López, Biotinylated selenocyanates: Potent and selective cytostatic agents, Bioorg. Chem. 133 (2023), 106410, https://doi.org/10.1016/j.bioorg.2023.106410.